Angewandte Chemie International Edition

Angewandte International Edition Chemie

How to cite: *Angew. Chem. Int. Ed.* **2026**, 65, e21595
doi.org/10.1002/anie.202521595

RESEARCH ARTICLE OPEN ACCESS

The Far Side of Carboranes: Anticancer Active Monocations and Ambiently Stable Dications

Vlastimil Němec[1] | Josef Holub[2] | Maksim A. Samsonov[1] | Zdeňka Růžičková[1] | Josef Cvačka[3] | Ján Vančo[4] | Zdeněk Trávníček[4] | Jan Belza[4,†] | Zdeněk Dvořák[5] | Jan Vrána[1] | Aleš Růžička[1]

[1]Department of General and Inorganic Chemistry, Faculty of Chemical Technology, University of Pardubice, Pardubice, Czech Republic | [2]Institute of Inorganic Chemistry, Czech Academy of Sciences, Řež, Czech Republic | [3]Institute of Organic Chemistry and Biochemistry, Czech Academy of Sciences, Flemingovo náměstí, Praha, Czech Republic | [4]Regional Centre of Advanced Technologies and Materials, Czech Advanced Technology and Research Institute, Palacký University, Olomouc, Czech Republic | [5]Department of Cell Biology and Genetics, Faculty of Sciences, Palacký University, Olomouc, Czech Republic

Correspondence: Jan Vrána (jan.vrana@upce.cz) | Aleš Růžička (ales.ruzicka@upce.cz)

Received: 2 October 2025 | **Revised:** 16 March 2026 | **Accepted:** 16 March 2026

Keywords: carborane cluster | cation | cellular effects | in vitro cytotoxicity | proton-coupled electron transfer

ABSTRACT

Polyhedral carboranes are highly biologically stable, non-toxic clusters. Whereas they are typically encountered in anionic or neutral forms, positively charged species have only recently been discovered. The in vitro antiproliferative effects of selected carboranes were assessed using a panel of human cancer cell lines, and off-target toxicity was evaluated at normal cell lines. The results demonstrated significant anticancer activity and a favorable resistance factor (RF ≈ 1) for monocationic carborane ***o*-2a**, surpassing the effects of *doxorubicin* and *cisplatin*. In pursuit of even more efficient substrates, the first dicationic polyhedral boranes were synthesized. These water-stable dications exhibit a reversible *closo*-/*nido*- cage opening, triggered either by a strong base (DMAP) or by a combination of triethylamine and molecular hydrogen, and reversed upon the addition of acid. The former transformation proceeds without a redox change, while the latter involves a $H_2/2H^+$ conversion in a proton-coupled electron process.

1 | Introduction

Polyhedral boranes and heteroboranes occupy a unique position at the intersection of inorganic and organic chemistry, showing reactivity reminiscent of both main-group hydrides and aromatic systems [1–3]. Due to the delocalization of electron density across the entire cluster, neutral and anionic (hetero)boranes possess exceptional thermal stability among molecular compounds. The small electronegativity difference between boron and hydrogen renders the B–H bond generally nonpolar yet capable of exhibiting either protic or hydridic character depending on the molecular structure.

With hundreds of structural motifs reported to date, boranes and heteroboranes have been extensively studied for applications in many areas such as energy storage and conversion, materials science, nuclear-waste remediation, and medicine [4–9]. Their medicinal potential is particularly promising owing to their low toxicity and high biological stability. Thanks to their steric and electronic properties, these clusters can act as phenyl mimetics, replacing organic moieties in various drugs, anticancer agents, and pharmacophores [10–19]. Their inherent hydrophobicity makes them ideal candidates for therapeutic and diagnostic labelling as well as radiotherapies such as BNCT [20–25], offering a significantly higher boron-atom content than non-cluster compounds.

Although hydrophobicity is often a desirable property, polyhedral boranes can be readily polarized through reduction to anionic species or functionalized with polar organic substituents

[†]Our beloved colleague and friend, who passed away unexpectedly on February 15, 2024, at the age of 31.

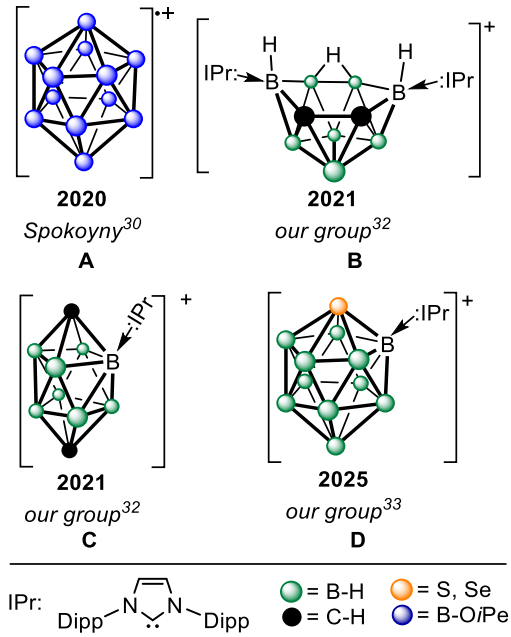

SCHEME 1 | An overview of published cationic boranes and heteroboranes. The *closo*-radical A is persubstituted with alkoxy groups, whereas the thermally robust heteroboranes are stabilized by bulky N-heterocyclic carbenes and adopt *pseudonido*- (B) or *closo*- (C and D) configurations. Dipp = 2,6-di*iso*propylphenyl.

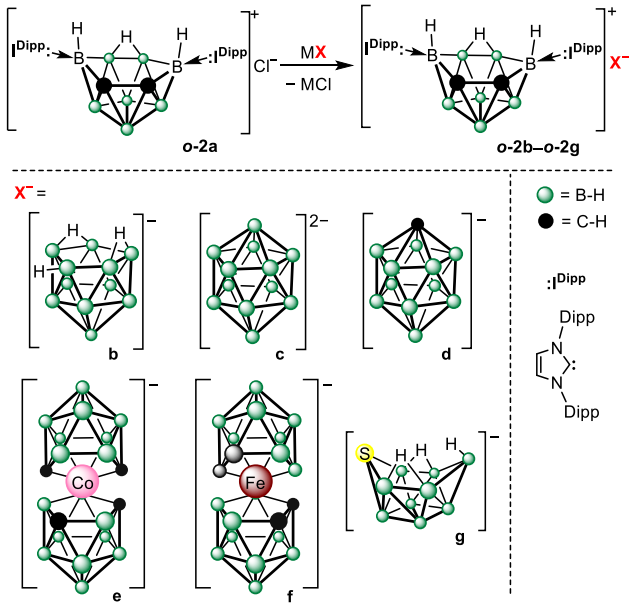

SCHEME 2 | The reactivity of the carborane ***o*-2a** with anionic polyhedral boranes and heteroboranes. The reactions proceed via simple metathesis, eliminating insoluble chlorides (MCl = NaCl, CsCl, and Et_3NHCl). Dipp = 2,6-di*iso*propylphenyl.

[26]. Conversely, oxidation to cationic species—which could dramatically alter borane properties such as lipophilic-cell-membrane permeability, acid stability, and aqueous solubility—has remained elusive until recently. Although many borane or heteroborane clusters occur as cationic components in molecules, the positive charge is typically localized on exoskeletal groups containing ammonium, phosphonium, or sulfonium moieties [27–29].

The first cationic borane was synthesized via stepwise oxidation of *closo*-$[B_{12}(OiPe)_{12}]^{2-}$ to the radical cation *closo*-$[B_{12}(OiPe)_{12}]^{\bullet+}$ (Scheme 1A) [30, 31]. The persubstitution of B–H moieties with bulky alkoxy groups proved insufficient for stability, because the radical decomposes above −30°C. The first thermally robust cationic heteroboranes were prepared from 10-vertex carboranes using complexes with bulky N-heterocyclic carbenes, which—despite being neutral—exhibited sufficient basicity to accept a proton of H–Cl, yielding cationic carboranes in *pseudonido*- (Scheme 1B) or *closo*-configurations (Scheme 1C) [32]. The presence of a positive charge within the cluster was confirmed both spectroscopically and computationally. Recently, we have demonstrated that this strategy can be extended to other heteroboranes, including chalcogenaboranes (Scheme 1D) [33]. These compounds represent unique examples not only within borane-cluster chemistry but also in group-13 chemistry in general, as recently reviewed [34].

Given the importance of radiotherapy in contemporary cancer treatment, we focused on boron cluster scaffolds, which intrinsically provide the highest attainable boron content. To date, BNCT agents bearing boranes and heteroboranes have relied predominantly on anionic compounds, including derivatives of $[B_{12}H_{12}]^{2-}$ and $[Co(C_2B_9H_{11})_2]^-$, which exhibit limited nucleophilicity despite their formal negative charge, or on neutral 12-vertex carboranes, mainly employed as biocompatible appendages or as aryl surrogates in established therapeutic scaffolds [10–19]. The lack of accessible cationic counterparts has effectively precluded exploration of charge-inverted architectures.

Herein, we exploit hydrolytically robust polyhedral cationic carboranes to interrogate the biological consequences of introducing a positive charge into the cluster framework. In parallel, we systematically evaluate the role of the counterion and targeted structural modifications in modulating both the chemical behaviour and biological performance of these species.

2 | Results and Discussion

2.1 | *o*-2a Metathesis

To this end, we investigated the chloride-anion exchange of ***o*-2a** with various polyhedral boranes and heteroboranes, assessing the stability of two oppositely polarized boranes within a single compound and seeking to increase further the boron-atom count per compound (Scheme 2). A diverse set of anionic counterparts was selected to represent different structural types of heteroboranes (*closo*-, *nido*-, and *arachno*-) as well as various heteroatoms and charges. The compounds ***o*-2b**–***o*-2g** were synthesized via simple metathesis, involving the elimination of insoluble salts (NaCl, CsCl, Et_3NHCl). To the best of our knowledge, these are the first reported examples of mixed ionic pairs of polyhedral boranes. The NMR spectra of ***o*-2b**–***o*-2g** showed no notable differences compared to those of the individual ions. The molecular structure of ***o*-2e** was confirmed by x-ray diffraction analysis (Figures S122–S124 also show structures of ***o*-2c** and ***o*-2d**, which contained considerable amount of solvent molecules, for more information see the Supporting Information), which revealed no significant

TABLE 1 | The results of antiproliferative-activity testing using the MTT method (24-h incubation).

Compound	Antiproliferative activity against human cancer and normal cell lines (IC_{50} ± SD)								
	A2780	**A2780R**	**PC3**	**A549**	**MCF7**	**HOS**	**HT-29**	**MRC5**	**HaCaT**
***o*-2a**	1.4 ± 0.3	1.3 ± 0.4	2.4 ± 0.1	5.0 ± 3.7	3.2 ± 0.1	2.5 ± 0.1	3.4 ± 0.5	2.7 ± 0.4	2.8 ± 0.5
Doxorubicin	2.1 ± 1.1	3.6 ± 0.2	>20	>20	3.7 ± 3.4	9.1 ± 3.9	>20	>20	n.t.
Cisplatin	17.2 ± 0.9	>50	>50	>50	33.0 ± 4.1	33.2 ± 4.4	>50	>50	>50

Note: The IC_{50} values (μM) were determined for the selected compounds and reference drugs (doxorubicin and cisplatin) on human cancer and normal cell lines. The values are presented as the means ± standard deviation (SD). n.t. = not tested. The complete table of cytotoxicity data is given in Table S15.
Ovarian carcinoma, A2780; cisplatin-resistant ovarian carcinoma, A2780R; prostate carcinoma, PC3; lung adenocarcinoma, A549; breast adenocarcinoma, MCF7; osteosarcoma, HOS; colorectal adenocarcinoma, HT-29; lung fibroblast, MRC5; aneuploid immortal keratinocyte, HaCaT. ***o*-2a** was also evaluated on the PANC1, CaCo2 and HeLa cancer cell lines, with IC_{50} values of 3.3 ± 0.2 μM, 13.9 ± 0.4 μM, and 2.7 ± 0.3 μM, respectively.

intermolecular interactions between the positively and negatively charged clusters—likely due to the delocalization of both positive and negative charges in the respective ions. Unfortunately, the compounds ***o*-2b**–***o*-2g** exhibited poor solubility in water (<< 1 mg/mL) and gradual decomposition in solution, leading us to focus biological-activity testing solely on the compound ***o*-2a**.

2.2 | The Evaluation of In Vitro Anticancer Activity

2.2.1 | In Vitro Antiproliferative Activity on a Panel of Human Cancer Lines and Normal Cells

The in vitro cytotoxicity of ***o*-2a** and $Cs[Co(1,7\text{-}C_2B_9H_{11})_2]$ (precursor of ***o*-2a**, labelled as ***pre*-*o*-2e**) was assessed in seven human cancer cell lines, with ***o*-2a** further tested in three additional lines. The results (Tables 1 and S15) showed that the monocationic ***o*-2a** displayed pronounced antiproliferative activity across all cancer cell lines, with IC_{50} values of 1.3–14.0 μM, generally surpassing reference drugs *doxorubicin* and *cisplatin* as well as other compounds tested in this work (see below). Selectivity was evaluated using normal MRC5 and HaCaT cells, with the selectivity index (SI) defined as the ratio of IC_{50} in non-cancerous to cancer cells. The most favorable SI values (SI≈2) were obtained for A2780 and A2780R. Importantly, ***o*-2a** exhibited a resistance factor (RF≈1), calculated as the IC_{50} ratio in A2780R/A2780 cells, which is superior to *cisplatin* (RF≈3), indicating promising activity against resistant cancer cell lines.

Based on the outcomes from antiproliferative activity tests using a 24-h incubation, we aimed to examine how incubation time affects the antiproliferative properties of ***o*-2a**. Consequently, the time-dependent antiproliferative activity (with incubation periods of 24, 48, and 72 h) was assessed using the A2780 cell line (see Table S16). These experiments showed a significant decrease in IC_{50} values for ***o*-2a**, reaching 1.6, 0.5, and 0.4 μM after 24, 48, and 72 h of incubation, respectively. The time-dependent cytotoxicity of *doxorubicin* and *cisplatin* displayed a typical decline in IC_{50} values over time.

2.2.2 | Cellular Effects of Selected Complexes Studied on Ovarian A2780 Cancer Cells

The effect of the tested compounds on the cell cycle of A2780 cells after 24-h incubation is shown in Figure 1a. The monocationic ***o*-2a** potently and significantly arrested A2780 cells in the G0/G1 phase (resting phase) and markedly decreased the cell populations in both the synthetic (S) and G2/M phases of the cell cycle, in contrast to *cisplatin*, which arrested most of the cells in the S phase. These results indicate a completely different mechanism of action for ***o*-2a** than for *cisplatin*. Following the cell-cycle analysis, a series of assays describing the ability of the compounds to induce cell-death processes was performed. Based on the results of the Annexin V/propidium iodide assay (Ann V/PI), the antiproliferative effect of ***o*-2a** cannot be ascribed to the induction of programmed cell death in A2780 cells (see Figure 1b). C*isplatin* caused significant damage to A2780 cells and initiated apoptosis in more than 30% of all cells.

These findings were further supported by the detection of the active executioner caspases Casp 3/7 in A2780 cells (see Figure 1c). Overall, these results imply that the antiproliferative effects of the studied carboranes may be related to the modulation of the metabolic activity of the target A2780 cells. To reinforce this hypothesis, we investigated the impact of ***o*-2a** on mitochondrial-membrane potential (see Figure 1d) and the induction of autophagy (for more details, see Figure S131). Autophagy is typically triggered by environmental stressors that negatively impact cellular metabolism. Nevertheless, ***o*-2a** showed no significant effects on the activation of autophagy in A2780 cells after 24 h of incubation. In contrast, as shown in Figure 1d, the most potent antiproliferative agent, ***o*-2a**, caused notable mitochondrial membrane depolarization, exceeding the effects of the reference platinum-based chemotherapeutic *cisplatin* and the positive control, carbonyl cyanide 3-chlorophenylhydrazone (CCCP), used at 50 μM. This unexpected, organelle-targeted activity of ***o*-2a** clearly disrupts the energetic metabolism of A2780 ovarian cancer cells and might represent a key mechanism behind its antiproliferative effect.

The loss of mitochondrial-membrane potential can be associated with the structural deterioration of the outer mitochondrial membrane, leading to uncontrolled permeation and the disruption of the proton gradient normally maintained across this membrane. These structural changes can be triggered by the direct damaging effects of reactive oxygen species (ROS), generated either as byproducts of mitochondrial metabolism and/or through depletion of endogenous intracellular antioxidant agents such as glutathione during oxidative stress. Nevertheless, ROS/superoxide-production analysis in A2780 cells (see Figure S133) revealed either no or a slight antioxidant response from the tested compound.

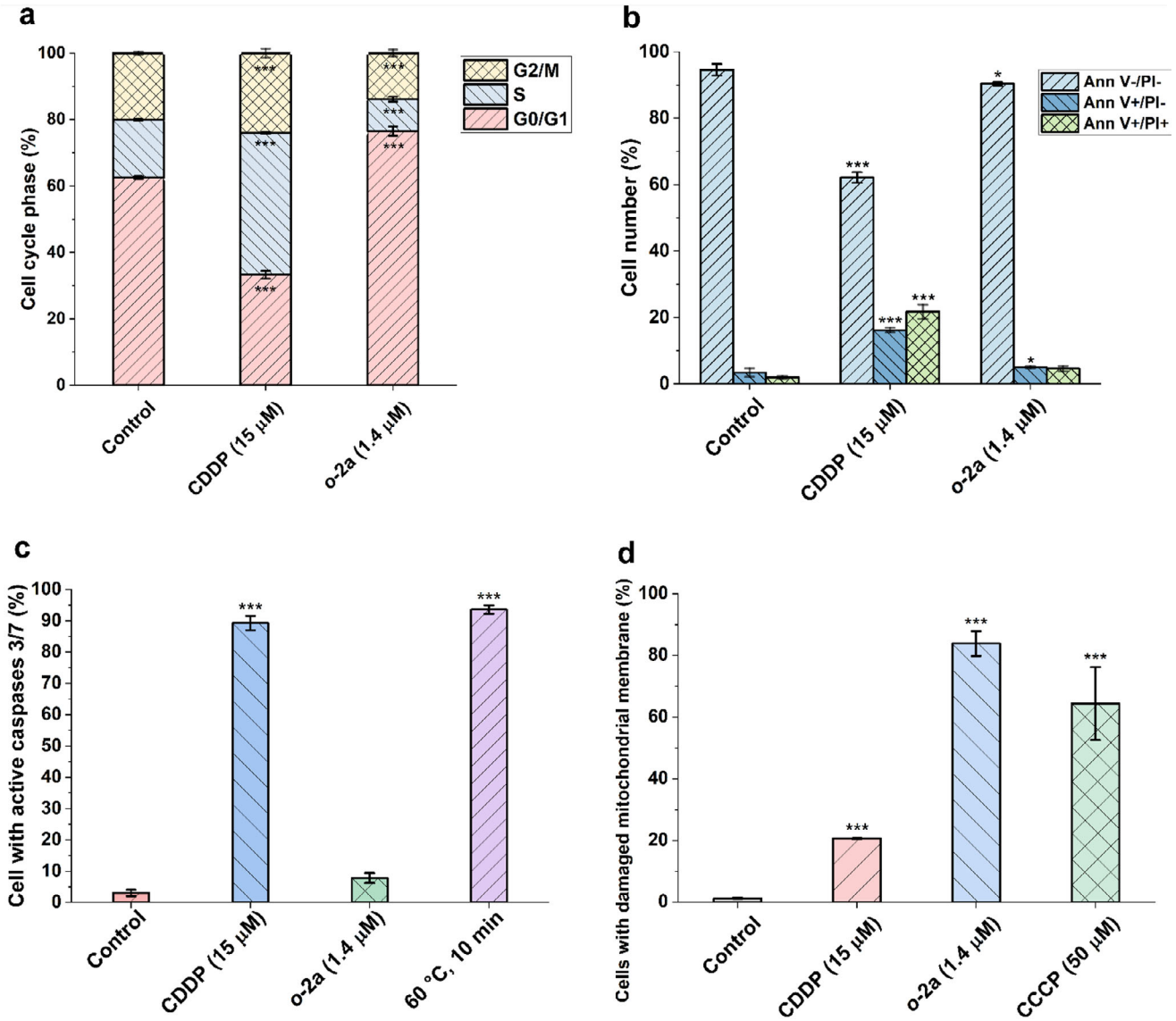

FIGURE 1 | Cellular effects of the tested compounds in A2780 cells. (a) The effects of the tested compounds on the cell cycle. (b) The induction of apoptosis/necrosis in the Annexin V/PI assay. (c) The activation of executioner caspases Casp 3/7. (d) The effect on the mitochondrial-membrane potential in A2780 cells after 24-h incubation using half-cytotoxic concentrations (based on MTT-assay results). Significance levels: *$p<0.05$, **$p<0.01$, ***$p<0.005$. *Note:* The complete data related to cellular effects are shown in Figure S132.

2.3 | Modification of the Tested Carborane *o*-2a

The observed cytotoxicity effectively precludes any application of ***o*-2a** in radiotherapy and necessitates structural modification of both the cluster core and the supporting carbene ligands. The most plausible origin of this cytotoxicity is insufficient stability under intracellular conditions. According to Wade's rules, ***o*-2a** adopts an *arachno*-type framework, which is the least stable toward hydrolysis in the *closo-* > *nido-* > *arachno*-series, despite exhibiting reasonable stability in aqueous media [1, 32]. In order to increase the stability of the positively charged carborane, we turned our attention to *closo*-carboranes. A single representative of this group (Scheme 1C) was prepared by reacting the carbene–carborane complex ***p*-2^{Dipp}** (Scheme 3) with hydrogen chloride, eliminating dihydrogen and imidazolium in the process. Although the reaction was nearly quantitative (based on the NMR spectra of the reaction mixture), the isolated yield was low due to the challenging separation from **I^{Dipp}**·HCl. Moreover, ***p*-2a^{Dipp}** exhibited lower solubility in water than ***o*-2a**. To reduce hydrophobicity, we thus employed N-heterocyclic carbenes (**:I^{iPr}** and **:I^{Cy}**, Scheme 3) bearing smaller organic substituents. The reaction of *p*-$C_2B_8H_{10}$ (***p***) with these carbenes yielded the expected carboranes ***p*-2^{iPr}** and ***p*-2^{Cy}** (Scheme 3), with significantly shortened reaction times from days to hours. This was attributable to the lower steric hindrance of **:I^{Cy}** and **:I^{iPr}**, because the reaction proceeds exclusively in a 1:2 ratio. However, the subsequent treatment of ***p*-2^{iPr}** and ***p*-2^{Cy}** with hydrogen chloride did not follow the same pathway as their bulkier analogue. Surprisingly, instead of eliminating one molecule of dihydrogen and imidazolium chloride, two molecules of dihydrogen were released, yielding the positively charged species ***p*-2a^{iPr}** and ***p*-2a^{Cy}** compensated by two chloride anions. Atomic charges in

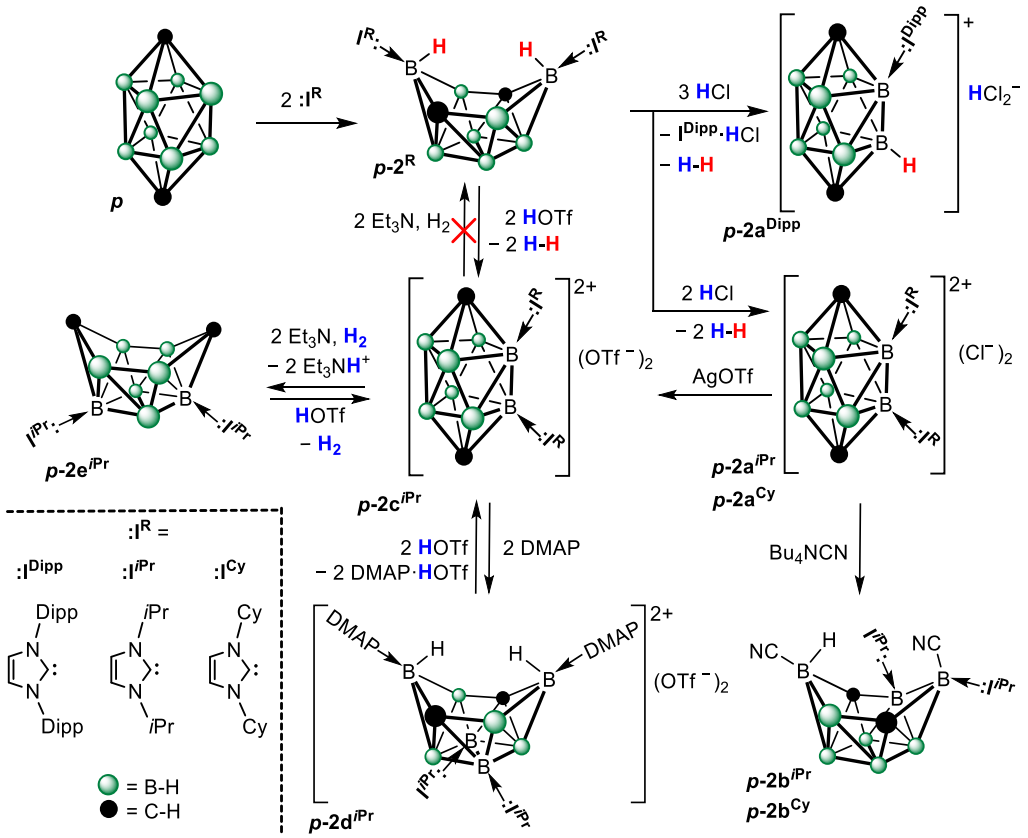

SCHEME 3 | The synthesis and reactivity of dicationic carboranes. The reaction of 1,10-$C_2B_8H_{10}$ (*p*) with the N-heterocyclic carbene **:I^{Dipp}** followed by treatment with hydrogen chloride, yields the monocationic ***p*-2a^{Dipp}** (previous work) [32], whereas **:I^{iPr}** and **:I^{Cy}** afford the dicationic species ***p*-2a^{iPr}** and ***p*-2a^{Cy}**. The dicationic carboranes ***p*-2a^{iPr}** and ***p*-2c^{iPr}** react with Bu_4NCN, DMAP, or triethylamine/H_2, resulting in the opening of the carborane cage irreversibly (***p*-2b^{iPr}**) or reversibly (***p*-2d^{iPr}** and ***p*-2e^{iPr}**), which can be reversed by the addition of an acid. Dipp = 2,6-di*iso*propylphenyl; Cy = cyclohexyl.

p*-2a^{iPr}** and ***p*-2a^{Cy}** were calculated using AIM analysis (Table S9), which revealed that the positive charge is predominantly localized within the carborane cage (1.399 and 1.398 e), while the carbenes are only slightly polarized (0.119–0.166 e). This contrasts with the previously reported clusters from the cationic group 13, where the positive charge is delocalized onto the donor bases, compensating for the cationic center [34]; for example, AIM analysis of tetracationic $[\{M(dmpe)\}_4]^{4+}$ (M = Ga, In; dmpe = 1,2-bis(dimethylphosphino)ethane) has estimated charges of only 0.28 (In) and 0.3 (Ga) e per metal atom [35]. A detailed analysis of individual skeletal atoms in ***p*-2a^{iPr}** and ***p*-2a^{Cy}** shows that the positive charge is evenly distributed across the entire cluster, with no boron atom more charged than the others (see ESI for details). This is further supported by the ^{11}B NMR spectra. Whereas the parent carborane ***p displays a single signal (−13 ppm), coordination of two carbene molecules lowers the symmetry, dramatically altering the electron distribution and resulting in a broad range of chemical shifts (between −44.5 and −6.6 ppm), which is typical for the *arachno*-shaped ten vertex clusters [36] and is nearly identical with the spectrum of ***p*-2^{Dipp}** [32]. In contrast, cage closure and formal oxidation to the dication restores the uniform electron distribution, with all boron signals appearing in a narrow range similar to the parent ***p*** (between −8 and −12 ppm). A similar situation was found for the skeletal carbon atoms, as their ^{13}C NMR shifts in ***p*** (103.3 ppm), and the dications (106.9 and 107.5 ppm) are strongly downfield-shifted compared to ***p*-2^{iPr}** and ***p*-2^{Cy}** (28.5 and 28.6 ppm) due to the antipodal effect [37]. These trends have also been observed previously for both monocationic carboranes and chalcogenaboranes [32, 33]. It is also consistent with the fact that these compounds retain their skeletal–electron-pair (SEP) count as ***p***. According to the Wade–Mingos rules [38–42], the number of SEPs in ***p*-2a^{iPr}** and ***p*-2a^{Cy}** corresponds to a *closo*-arrangement, because the formal reduction by carbenes and subsequent oxidation connected via proton-coupled electron transfer (the protons are formally reduced to dihydrogen molecule) do not alter the SEP count within the cluster, as previously described for chalcogenaboranes [33]. The carboranes ***p*-2a^{iPr}** and ***p*-2a^{Cy}** represent unique examples among group-13 dications. The delocalization of charge throughout the cluster significantly enhances their stability, allowing them to be handled without an inert atmosphere and to be readily dissolved in water and methanol without decomposition for at least 1 month. In contrast, other group-13 dicationic compounds are typically sensitive to moisture and oxygen and often require stabilization by weakly coordinating anions [34, 43].

The molecular structures of ***p*-2a^{iPr}** and ***p*-2a^{Cy}** were confirmed by x-ray diffraction analysis, revealing a *closo*-arrangement for both dications, with B–B and B–C bond lengths falling within narrow ranges (Figures 2 and S126). Crystallization of ***p*-2a^{Cy}** from undried dichloromethane resulted in the formation of a rare complex counteranion, $[(H_3O)Cl_3]^{2-}$. Its formation is most likely

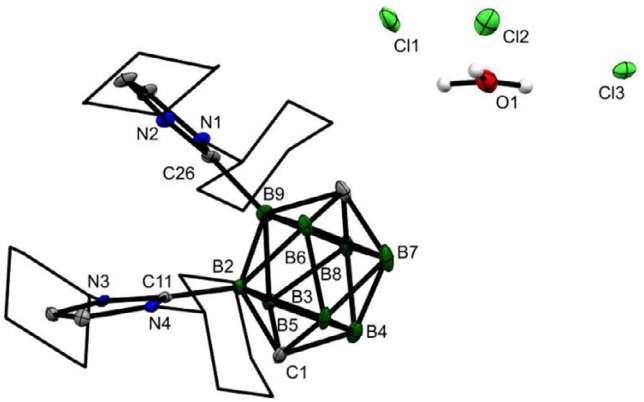

FIGURE 2 | The molecular structure of ***p*-2a^{Cy}**. The ORTEP diagrams are shown at a 40% probability level; the Cy groups are displayed as wireframes for clarity. Solvent molecules have been omitted. Selected interatomic distances [Å]: B–B: 1.796(13)–1.879(12), C1–B: 1.594(13)–1.612(11), C10–B: 1.591(13)–1.612(11), B2–C11: 1.580(11), B9–C26: 1.594(11), Cl1–O1: 2.884(6), Cl2–O1: 2.891(6), Cl3–O1: 2.905(6).

a consequence of the absence of direct interactions between chloride ions and the dication, because the delocalized positive charge within the cluster is efficiently shielded by hydride atoms and carbene ligands. To the best of our knowledge, this arrangement has been published previously three times [44–46], as usually $[H_3OCl_2]^-$ or its dimer $[H_6O_2Cl_4]^{2-}$ are produced [47]. The chloride atoms are linked with the pyramidalized oxonium cation via hydrogen bonding with separations (2.026–2.166) closer to the sum of covalent radii rather than van der Waals ($\Sigma_{vdW} = 3.02$; $\Sigma_{vdW} = 1.31$), which coincides with the earlier reports. Interestingly, it is impossible to dissolve the dications in dried aprotic solvents such as dichloromethane or acetonitrile; however, the addition of water inflicts a partial solubility, apparently due to the solvation of the chloride anions. On the contrary, the insolubility was practically used to wash ***p*-2a^{iPr}** and ***p*-2a^{Cy}** from impurities and enabled smooth multi-gram scale synthesis.

To shed more light on the formation of dicationic species, the mechanisms of the reactions of ***p*-2^{iPr}** and ***p*-2^{Dipp}** with hydrogen chloride have been investigated computationally (Figure S129) at the B3LYP/def2-TZVP level of theory using the PCM solvation model (tetrahydrofuran). The SMD model was also tested and yielded similar relative energies (Table S11), with no notable differences in the structures of intermediates and transition states. The first step, which is identical for both reactions, involves coordination of a hydrogen chloride molecule followed by proton transfer to a bridging position (B1–H1–B2, INT-1). Subsequent elimination of a dihydrogen molecule (TS-2) leads to the formation of a monocationic intermediate (INT-2). From this point, the mechanism diverges depending on the steric properties of the carbene. In the case of bulky **:I^{Dipp}** (Dipp groups, red path), the most thermodynamically favorable route involves cage closure to ***p*-2a^{Dipp}**, accompanied by the elimination of the carbene, which likely reacts with another equivalent of hydrogen chloride to form an imidazolium salt. Notably, this transition state (TS3′) corresponds to a *Z*-rearrangement [48] previously described for ten-vertex boranes and carboranes. In contrast, the less sterically hindered carbenes **:I^{iPr}** allow the introduction of a second hydrogen–chloride molecule (INT-3) and the elimination of dihydrogen (TS-4) prior to the cage closure. The resulting open dicationic form (TS-5) is immediately reclosed to ***p*-2a^{iPr}**, consistent with the Z-rearrangement. To assess the energetic feasibility of alternative products theoretically, we modeled hypothetical mono(di)cationic compounds ***p*-2a^{Dipp*}** and ***p*-2a^{iPr*}** with mixed carbene substituents (see, Figure S130). The calculated Gibbs free energies (ΔGr) of these species (6.93 and 2.29 kcal/mol) suggest that their formation is energetically disfavored with respect to ***p*-2a^{Dipp}** and ***p*-2a^{iPr}** (−37.40 and −35.64 kcal/mol) and thus unlikely.

We have evaluated the in vitro antiproliferative effects of the dicationic compounds ***p*-2a^{iPr}** and ***p*-2a^{Cy}**, which, in contrast to the monocationic ***o*-2a**, were inactive up to their solubility limits, except for ***p*-2a^{Cy}**, which showed moderate activity (IC_{50} = 11.6 μM) in A2780 and A2780R cells. This might be attributed to their higher stability provided by the *closo*-arrangement, as we have expected. The low cytotoxicity makes them more suitable for potential radiotherapy studies compared to ***o*-2a**. The stabilizing effect of the *closo*-arrangement outweighs the increased polarity of the doubly charged carboranes, resulting in higher stability both in aqueous solution and in cellular environments. Notably, the steric bulk of the carbene substituents appears to have a lower impact on the overall stability of the cationic clusters. Although carboranes ***p*-2a^{iPr}** and ***p*-2a^{Cy}** have the same number of skeletal electron pairs (SEPs) as compound ***p***, their electrophilicity should be enhanced, as demonstrated by the reactivity of selenaboranes with weak bases such as sodium iodide and 2,6-di*iso*propylaniline [33]. It was thus a logical step to test the similar reactivity of dicationic species. Even in protic solvents (water and methanol), no reaction with halogens (Bu_4NX, X = Br, I) was observed, prompting us to explore more reactive pseudohalogens (Bu_4NX, X = NCS, CN, N_3). While thiocyanate left ***p*-2a^{iPr}** and ***p*-2a^{Cy}** intact, two cyanide anions opened the cluster to form neutral ***p*-2b^{iPr}** and ***p*-2b^{Cy}** (Scheme 3). This reaction proceeded even at low temperatures, in contrast to conventional cyanation of borane clusters, which typically requires elevated temperatures and/or transition-metal catalysts [49–52]. A plausible mechanism involves initial coordination of a cyanide to atom B5, followed by cage opening (Figure S127). A second cyanide then coordinates to one of the carbene-bearing boron atoms, yielding ***p*-2b^{iPr}** or ***p*-2b^{Cy}**. Unfortunately, ***p*-2b^{Cy}** could not be isolated from the reaction mixture due to a similar solubility with the reaction byproducts; however, its molecular structure has been confirmed by x-ray diffraction analysis (Figure 3).

Similarly, we tested the reaction with azide. The ^{11}B NMR spectrum of the reaction mixture revealed multiple species with patterns resembling ***p*-2b^{iPr}**, suggesting the formation of several isomers. This is not surprising considering the number of reactive boron atoms exposed upon cage opening.

In the early 2000s, main-group compounds in unusual oxidation states gained attention as transition-metal mimetics due to their ability to activate small molecules such as hydrogen and carbon dioxide [53]. Comparable chemistry has not been described for polyhedral boranes, except in cases involving reactivity at exoskeletal functional groups [54]. Since the reaction of ***p*-2^{iPr}** with hydrogen chloride to ***p*-2a^{iPr}** released elemental hydrogen, we hypothesized that base-induced rehydrogenation could establish a cycle of dihydrogen activation.

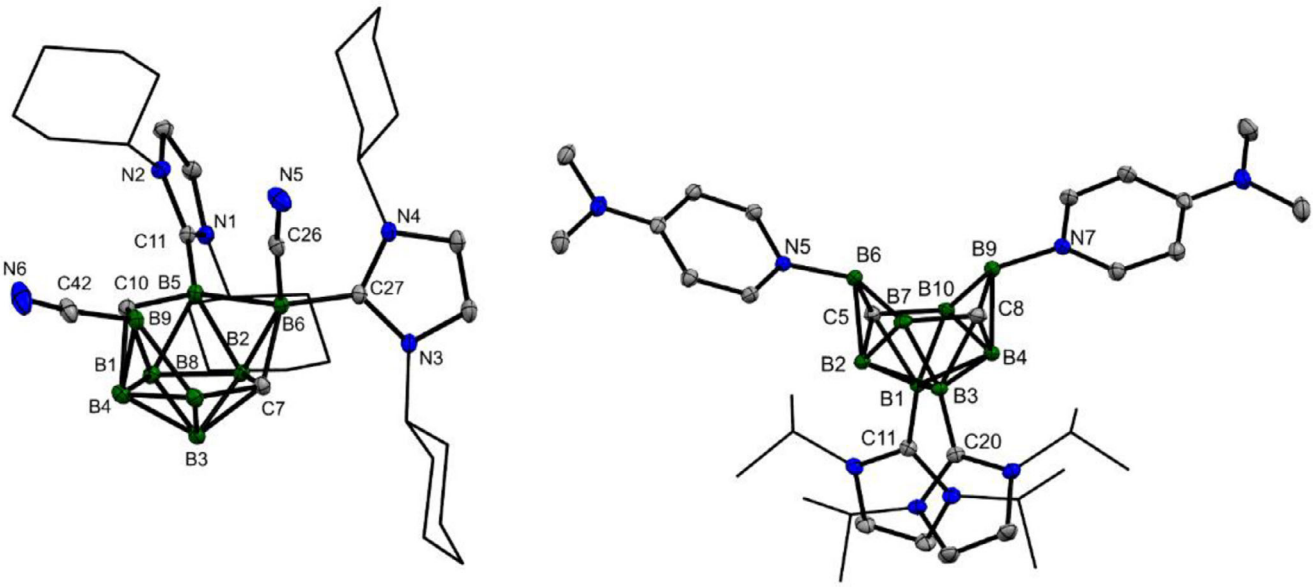

FIGURE 3 | The molecular structures of ***p*-2b^{Cy}** and ***p*-2d^{iPr}**. The ORTEP diagrams are shown at a 40% probability level; the *i*Pr and Cy groups are displayed as wireframes for clarity. Solvent molecules and anions have been omitted. Selected interatomic distances [Å]: ***p*-2b^{Cy}** B9–C42: 1.569(5), B6–C26: 1.579(5), C42–N6: 1.143(6), C26–N5: 1.151(5), B5–C11: 1.569(5), B6–C27: 1.655(5), B8–B9: 1.853(6), B9–C10: 1.635(5), C10–B5: 1.618(5), B5–B6: 1.924(6), B6–C7: 1.690(5), C7–B8: 1.609(5); ***p*-2d^{iPr}** N5–B6: 1.572(2), N7–B9: 1.573(2), C5–B6: 1.758(2), B6–B7: 1.742(2), B7–C8: 1.619(2), C8–B9: 1.711(2), B9–B10: 1.791(2), B10–C5: 1.600(2).

To test this, dication ***p*-2a^{iPr}** was treated with triethylamine and DMAP, but both reactions led to decomposition of the compound in both water and methanol, with visible gas evolution. To avoid protic solvents, we replaced chloride with triflate via metathesis using AgOTf, yielding ***p*-2c^{iPr}**, which is soluble in acetonitrile and can also be prepared directly by treating ***p*-2^{iPr}** with triflic acid. These findings are consistent with the results of the ***o*-2a** metathesis study, which demonstrated that pairing a sterically demanding cation with a small anion is optimal for stability in protic environments, whereas incorporation of a larger anion reduces lattice energy and thereby enhances solubility in less polar solvents. The subsequent reaction with DMAP produced ***p*-2d^{iPr}**. It strongly resembled the reaction of ***p*** with **:I^{iPr}** and resulted in cage opening to a *pseudonido*-arrangement via the *Z*-rearrangement (Figure S128), described above. Unlike the reaction with cyanide, this transformation began at atom B4, opposite the carbene-bearing vertex B2, most likely due to steric factors.

The carborane ***p*-2d^{iPr}** shares structural features with ***p*-2^{iPr}** but remains positively charged due to the loss of two hydrogen atoms. To compare their chemical behavior, we treated ***p*-2d^{iPr}** with hydrogen chloride (triflic acid), but the more polarized B–N bond proved weaker than the B—C(carbene) bond and was readily quenched, generating ***p*-2a^{iPr}** (***p*-2c^{iPr}**). The reaction with triethylamine, a considerably weaker base, did not proceed under strict anhydrous conditions. However, triethylamine must be capable of activating the dication, as decomposition has been observed in protic solvents.

Therefore, we repeated the reaction with triethylamine under a hydrogen atmosphere (1.5 bar), successfully obtaining the hydrogenation product ***p*-2e^{iPr}**, formed via hydrogenation to a *nido*-shaped cluster, followed by deprotonation. Notably, the same reaction did not proceed without triethylamine, whose presence is essential for proton removal, as demonstrated by the reverse reaction of ***p*-2e^{iPr}** with triflic acid, which smoothly regenerated the dicationic ***p*-2c^{iPr}**. Unfortunately, ***p*-2e^{iPr}** was obtained in low yield due to the over-hydrogenation of the dicationic ***p*-2c^{iPr}**, as evidenced by the ^{11}B NMR spectrum of the reaction mixture, which showed various hydrogenation products, including the $Et_3N–BH_3$ complex.

To the best of our knowledge, the only comparable hydrogenation of a *closo*-borane is that of $B_{10}H_{10}^{2-}$, which reacts with strong protic acids to form the *nido*-type complexes 6,9-$L_2B_{10}H_{12}$ (L = Et_2S, CH_3CN) [55]. This reaction is reversible upon base addition, regenerating $B_{10}H_{10}^{2-}$. The opening and closing patterns of both clusters are similar, as they retain the same SEP count, but the polarity is inverted—from 2+ (***p*-2a^{iPr}**) to 2– ($B_{10}H_{10}^{2-}$) in the *closo*-compounds–which is, to the best of our knowledge, the largest polarity difference between two isostructural boranes reported to date. Notably, this process involves a redox couple ($H_2/2H^+$), whereas the decaborate system undergoes simple proton exchange.

We did not observe similar hydrogenation of the monocationic ***p*-2a^{Dipp}** (Scheme 3), likely due to its lower electrophilicity. This is reflected in the HOMO–LUMO-gap values, which decrease in the order ***p*** > ***p*-1a^{Dipp}** > ***p*-2a^{iPr}** (7.29, 3.31, and 2.22 eV, respectively; see Table S10 for details).

The ^{11}B NMR spectra of the opened carboranes revealed expected patterns in a broad range of chemical shifts (−4.2–(−44.2) ppm) corresponding to *arachno*- (***p*-2b^{iPr}** and ***p*-2d^{iPr}**) and *nido*- (***p*-2e^{iPr}**) type clusters. Differences between the respective cluster arrangements are clearly shown in the correlation diagram (Figure 4, for more information see Supporting Information,

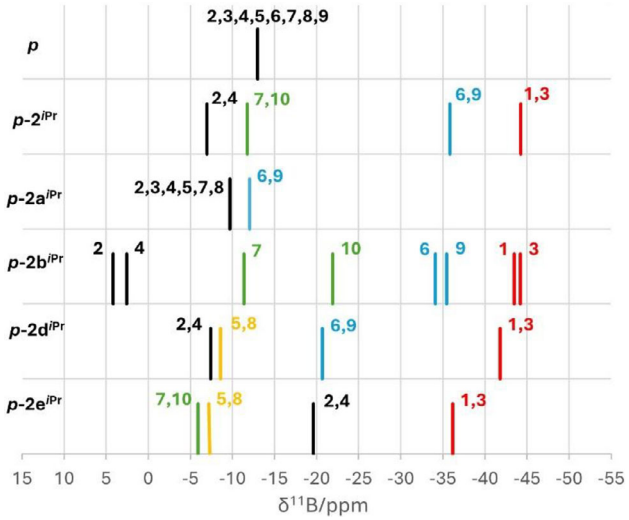

FIGURE 4 | Correlation diagram of ^{11}B NMR spectra of the carborane *p*-$C_2B_8H_{10}$ (***p***) and prepared compounds. The *closo*-carboranes ***p*** and ***p*-2a^{iPr}** exhibit signals around −11 ppm, whereas the *nido*- and *arachno*- are distributed in a broad range.

Table S1). The shifts of individual positions in the ^{11}B spectra vary only with the change of substituents (typically hydrogen–carbene substitution).

3 | Conclusion

A series of high-boron-content ionic carboranes has been synthesized via the ion exchange of various borane and heteroborane clusters. Among them, the cationic carborane ***o*-2a** exhibited notable antiproliferative activity, outperforming classic anticancer agents such as *doxorubicin* and *cisplatin*. Targeting the applications of the positively charged clusters in BNCT, we started to explore structural modifications of ***o*-2a**, moving toward a more stable *closo*-arrangement. The elusive dicationic carboranes ***p*-2a^{iPr}** and ***p*-2a^{Cy}** were prepared through formal reduction of the 10-vertex carborane ***p*** to *nido*-type complexes, followed by cage closure via formal oxidation with hydrogen chloride—in the end, without altering the SEP count in the *closo*-carboranes. Unlike other group-13 dications, ***p*-2a^{iPr}** and ***p*-2a^{Cy}** retain most of their positive charge within the cluster, as confirmed by theoretical calculations and spectroscopic data. Despite their high charge, both dications are air-stable and water-soluble, showing no decomposition after 1 month. Their stability was also reflected in their low antiproliferative activity, which makes them suitable candidates for BNCT studies. The enhanced electrophilicity is demonstrated by their uncatalyzed reaction with cyanide, which proceeds rapidly even at ambient temperature. The dicationic triflate ***p*-2c^{iPr}** undergoes reversible opening with DMAP and recloses upon acid treatment. Interestingly, reaction with triethylamine and molecular hydrogen does not yield the expected precursor ***p*-2^{iPr}** but its isomer ***p*-2e^{iPr}**, which can also be reclosed by acid. This reversible transformation involves a redox couple (H_2/$2H^+$) and suggests potential for dihydrogen activation–an uncommon feature among polyhedral boranes (excluding exoskeletal reactivity). Such proton-coupled electron transfer transformations are involved in many challenging reductions ranging from organic substrates to elemental nitrogen [56, 57].

Acknowledgments

The work was supported by ERC-CZ (project No. LL2309) and the Czech Science Foundation (Grant Number. 22-03945S).

Open access publishing facilitated by Univerzita Pardubice, as part of the Wiley - CzechELib agreement.

Conflicts of Interest

The authors declare no conflicts of interest.

Data Availability Statement

The raw NMR data of this study are openly available in Figshare.com at https://doi.org/10.6084/m9.figshare.30084781.

References

1. R. N. Grimes, *Carboranes*, 3rd ed. (Academic Press, 2016).

2. N. S. Hosmane, *Boron Science: New Technologies and Applications* (CRC Press, 2012).

3. D. Hnyk and M. McKee, *Boron: The Fifth Element*, 1st ed. (Springer International Publishing, 2015).

4. S. P. Fisher, A. W. Tomich, S. O. Lovera, et al., "Nonclassical Applications of Closo-Carborane Anions: From Main Group Chemistry and Catalysis to Energy Storage," *Chemical Reviews* 119 (2019): 8262–8290, https://doi.org/10.1021/acs.chemrev.8b00551.

5. N. S. Hosmane and R. Eagling, *Handbook of Boron Science With Applications in Organometallics, Catalysis, Materials and Medicine: Boron in Materials Chemistry* (World Scientific Publishing Company, 2018).

6. J. Brynda, P. Mader, V. Šícha, et al., "Carborane-Based Carbonic Anhydrase Inhibitors," *Angewandte Chemie International Edition* 52 (2013): 13760–13763, https://doi.org/10.1002/anie.201307583.

7. N. S. Hosmane and R. Eagling, *Handbook of Boron Science With Applications in Organometallics, Catalysis, Materials and Medicine: Boron in Medicine* (World Scientific Publishing, 2018).

8. E. Hey-Hawkins and C. Viñas Teixidor, *Boron-Based Compounds: Potential and Emerging Applications in Medicine* (Wiley, 2018), https://doi.org/10.1002/9781119275602.

9. R. J. Grams, W. L. Santos, I. R. Scorei, et al., "The Rise of Boron-Containing Compounds: Advancements in Synthesis, Medicinal Chemistry, and Emerging Pharmacology," *Chemical Reviews* 124 (2024): 2441–2511, https://doi.org/10.1021/acs.chemrev.3c00663.

10. J. F. Valliant, P. Schaffer, K. A. Stephenson, and J. F. Britten, "Synthesis of Boroxifen, a Nido-Carborane Analogue of Tamoxifen," *Journal of Organic Chemistry* 67 (2002): 383–387, https://doi.org/10.1021/jo0158229.

11. C. Selg, W. Neumann, P. Lönnecke, E. Hey-Hawkins, and K. Zeitler, "Carboranes as Aryl Mimetics in Catalysis: A Highly Active Zwitterionic NHC-Precatalyst," *Chemistry* 23 (2017): 7932–7937, https://doi.org/10.1002/chem.201700209.

12. C. Selg, A. Schöler, J. Schliehe-Diecks, et al., "Borinostats: Solid-Phase Synthesis of Carborane-Capped Histone Deacetylase Inhibitors With a Tailor-Made Selectivity Profile," *Chemical Science* 12 (2021): 11873–11881, https://doi.org/10.1039/D1SC02268G.

13. G. R. Kracke, M. R. Vangordon, Y. V. Sevryugina, et al., "Carborane-Derived Local Anesthetics Are Isomer Dependent," *Chemmedchem* 10 (2015): 62–67, https://doi.org/10.1002/cmdc.201402369.

14. M. Scholz, K. Bensdorf, R. Gust, and E. Hey-Hawkins, "Asborin: The Carbaborane Analogue of Aspirin," *Chemmedchem* 4 (2009): 746–748, https://doi.org/10.1002/cmdc.200900072.

15. C. Selg, T. Grell, A. Brakel, P. C. Andrews, R. Hoffmann, and E. Hey-Hawkins, "Fusing Bismuth and Mercaptocarboranes: Design and Biological Evaluation of Low-Toxicity Antimicrobial Thiolato

Complexes," *ChemPlusChem* 89 (2024): e202300759, https://doi.org/10.1002/cplu.202300759.

16. W. Neumann, S. Xu, M. B. Sárosi, et al., "nido -Dicarbaborate Induces Potent and Selective Inhibition of Cyclooxygenase-2," *Chemmedchem* 11 (2016): 175–178, https://doi.org/10.1002/cmdc.201500199.

17. P. Stockmann, L. Kuhnert, W. Leinung, et al., "Carboranes as Potent Phenyl Mimetics: A Comparative Study on the Reversal of ABCG2-Mediated Drug Resistance by Carboranylquinazolines and Their Organic Isosteres," *ChemMedChem* 19 (2024): e202300506, https://doi.org/10.1002/cmdc.202300506.

18. S. Sonam, S. Jelača, M. Laube, et al., "Carborane Conjugates With Ibuprofen, Fenoprofen and Flurbiprofen: Synthesis, Characterization, COX Inhibition Potential and in Vitro Activity," *Chemmedchem* 20 (2025): e202400018, https://doi.org/10.1002/cmdc.202400018.

19. C. Selg, V. Gordić, T. Krajnović, et al., "Re-Design and Evaluation of Diclofenac-Based Carborane-Substituted Prodrugs and Their Anti-Cancer Potential," *Scientific Reports* 14 (2024): 30488, https://doi.org/10.1038/s41598-024-81414-x.

20. P. Stockmann, M. Gozzi, R. Kuhnert, M.-B. Sárosi, and E. Hey-Hawkins, "New Keys for Old Locks: Carborane-Containing Drugs as Platforms for Mechanism-Based Therapies," *Chemical Society Reviews* 48 (2019): 3497–3512, https://doi.org/10.1039/C9CS00197B.

21. S. Kulkarni, D. Bhandary, Y. Singh, V. Monga, and S. Thareja, "Boron in Cancer Therapeutics: An Overview," *Pharmacology & Therapeutics* 251 (2024): 108548, https://doi.org/10.1016/j.pharmthera.2023.108548.

22. C. Alamón, B. Dávila, M. F. García, et al., "A Potential BNCT Agent Selectively Suppresses High-Grade Glioma: In Vitro and in Vivo Exploration," *Molecular Pharmaceutics* 20 (2013): 2702–2713.

23. I. Fuentes, T. García-Mendiola, S. Sato, et al., "Metallacarboranes on the Road to Anticancer Therapies: Cellular Uptake, DNA Interaction, and Biological Evaluation of Cobaltabisdicarbollide $[COSAN]^-$," *Chemistry – A European Journal* 24 (2018): 17239–17254, https://doi.org/10.1002/chem.201803178.

24. M. Couto, C. Alamón, S. Nievas, et al., "Bimodal Therapeutic Agents against Glioblastoma, One of the Most Lethal Forms of Cancer," *Chemistry – A European Journal* 26 (2020): 14335–14340, https://doi.org/10.1002/chem.202002963.

25. M. Nuez-Martínez, M. Queralt-Martín, A. Muñoz-Juan, et al., "Boron Clusters (ferrabisdicarbollides) Shaping the Future as Radiosensitizers for Multimodal (chemo/radio/PBFR) Therapy of Glioblastoma," *Journal of Materials Chemistry B* 10 (2022): 9794–9815, https://doi.org/10.1039/D2TB01818G.

26. R. Frank, V. Ahrens, S. Boehnke, et al., "Carbaboranes—More Than Just Phenyl Mimetics," *Pure and Applied Chemistry* 87 (2015): 163–171, https://doi.org/10.1515/pac-2014-1006.

27. E. J. M. Hamilton, H. T. Leung, R. G. Kultyshev, X. Chen, E. A. Meyers, and S. G. Shore, "Unusual Cationic Tris(Dimethylsulfide)-Substituted *Closo*-Boranes: Preparation and Characterization of $[1,7,9\text{-}(Me_2S)_3\text{-}B_{12}H_9]BF_4$ and $[1,2,10\text{-}(Me_2S)_3\text{-}B_{10}H_7]BF_4$," *Inorganic Chemistry* 51 (2012): 2374–2380, https://doi.org/10.1021/ic2023709.

28. J. A. Ioppolo, J. K. Clegg, and L. M. Rendina, "Dicarba-closo-dodecaborane(12) Derivatives of Phosphonium Salts: Easy Formation of Nido-Carborane Phosphonium Zwitterions," *Dalton Transactions* 20 (2007): 1982, https://doi.org/10.1039/b700689f.

29. A. Kataki-Anastasakou, J. C. Axtell, S. Hernandez, et al., "Carborane Guests for Cucurbit[7]uril Facilitate Strong Binding and On-Demand Removal," *Journal of the American Chemical Society* 142 (2020): 20513–20518, https://doi.org/10.1021/jacs.0c09361.

30. J. M. Stauber, J. Schwan, X. Zhang, et al., "A Super-Oxidized Radical Cationic Icosahedral Boron Cluster," *Journal of the American Chemical Society* 142 (2020): 12948–12953, https://doi.org/10.1021/jacs.0c06159.

31. A. I. Wixtrom, Y. Shao, D. Jung, et al., "Rapid Synthesis of Redox-active Dodecaborane $B_{12}(OR)_{12}$ Clusters Under Ambient Conditions," *Inorganic Chemistry Frontiers* 3 (2016): 711–717, https://doi.org/10.1039/C5QI00263J.

32. J. Vrána, J. Holub, M. A. Samsonov, et al., "Access to Cationic Polyhedral Carboranes via Dynamic Cage Surgery With N-Heterocyclic Carbenes," *Nature Communications* 12 (2021): 4971, https://doi.org/10.1038/s41467-021-25277-0.

33. J. Holub, Š.-P. Náhlík, Z. Růžičková, et al., "Cationic Polyhedral Chalcogenaboranes: Activation Without Breaking Wade's Rules," *Angewandte Chemie International Edition* 137 (2025): e202419677, https://doi.org/10.1002/ange.202419677.

34. A. Barthélemy and I. Krossing, "Cationic Group 13 and 14 Element Clusters," *Inorganic Chemistry* 63 (2024): 21763–21787, https://doi.org/10.1021/acs.inorgchem.4c03251.

35. A. Barthélemy, H. Scherer, and I. Krossing, "Direct Comparison of Subvalent, Polycationic Group 13 Cluster Compounds: Lessons Learned on Isoelectronic DMPE Substituted Gallium and Indium Tetracation Salts," *Chemistry – A European Journal* 28 (2022): e202201369, https://doi.org/10.1002/chem.202201369.

36. M. Bakardjiev, B. Štíbr, J. Holub, et al., "Sequential Camouflage of the *Arachno*-$6,9\text{-}C_2B_8H_{14}$ Cage by Substituents," *Inorganic Chemistry* 55, no. 14 (2016): 7068–7074, https://doi.org/10.1021/acs.inorgchem.6b00964.

37. M. Buehl, P. R. Schleyer, Z. Havlas, D. Hnyk, and S. Hermanek, "On the Origin of the Antipodal Effect in Closo-Heteroboranes," *Inorganic Chemistry* 30, no. 15 (1991): 3107–3111, https://doi.org/10.1021/ic00015a035.

38. R. E. Williams, "Carboranes and Boranes; Polyhedra and Polyhedral Fragments," *Inorganic Chemistry* 10 (1971): 210–214, https://doi.org/10.1021/ic50095a046.

39. K. Wade, "The Structural Significance of the Number of Skeletal Bonding Electron-Pairs in Carboranes, the Higher Boranes and Borane Anions, and Various Transition-Metal Carbonyl Cluster Compounds," *Journal of the Chemical Society D: Chemical Communications* 15 (1971): 792, https://doi.org/10.1039/c29710000792.

40. R. W. Rudolph, "Boranes and Heteroboranes: A Paradigm for the Electron Requirements of Clusters?," *Accounts of Chemical Research* 9 (1976): 446–452, https://doi.org/10.1021/ar50108a004.

41. D. M. P. Mingos, "Polyhedral Skeletal Electron Pair Approach. A Generalised Principle for Condensed Polyhedra," *Journal of the Chemical Society, Chemical Communications* 12 (1983): 706, https://doi.org/10.1039/c39830000706.

42. D. M. P. Mingos, "Polyhedral Skeletal Electron Pair Approach," *Accounts of Chemical Research* 17 (1984): 311–319, https://doi.org/10.1021/ar00105a003.

43. W. E. Piers, S. C. Bourke, and K. D. Conroy, "Borinium, Borenium, and Boronium Ions: Synthesis, Reactivity, and Applications," *Angewandte Chemie International Edition* 44 (2005): 5016–5036, https://doi.org/10.1002/anie.200500402.

44. M. S. Abdelbassit, O. J. Curnow, and M. R. Waterland, "Halocyclopropenium-Halide Halogen-Bonded Ion Pairs and Their Hydrogen-Bonded Halide Solvates," *Helvetica Chimica Acta* 106 (2023): e202200163, https://doi.org/10.1002/hlca.202200163.

45. G. R. Willey, T. J. Woodman, U. Somasundaram, D. R. Aris, and W. Errington, "Azamacrocyclic Stabilisation of the Halogenocations MX_3^+ Where M = Ge or Sn and X = Cl or Br. Synthesis and Molecular Structures of $[GeCl_3(L^1)]^+{}_2[H_3O]^+Cl^-{}_3\cdot MeCN$, $[SnCl_3(L^1)]^+{}_2[SnCl_6]_2^-\cdot 4MeCN$, $[GeBr_3(L_2)]^+{}_2[MeNH_3]^+Br^-{}_3\cdot MeCN$ and $[SnBr_3(L_2)]^+{}_2[SnBr_6]^{2-}$ Where L^1 = 1,4,7-Trimethyl-1,4,7-Triazacyclononane and L^2 = 1,3,5-Trimethyl-1,3,5-Triazacyclohexane," *Journal of the Chemical Society, Dalton Transactions* (1998): 2573–2576, https://doi.org/10.1039/a803175d.

46. R. M. Denton, J. An, B. Adeniran, A. J. Blake, W. Lewis, and A. M. Poulton, "Catalytic Phosphorus(V)-Mediated Nucleophilic Substitution Reactions: Development of a Catalytic Appel Reaction," *Journal of Organic Chemistry* 76 (2011): 6749–6767, https://doi.org/10.1021/jo201085r.

47. P. Bertocco, C. Bolli, B. A. Correia Bicho, C. Jenne, and M. C. Nierstenhöfer, "Insights Into the Structure of Halide-Rich Hydrochloric and Hydrobromic Acid: A Structural and Quantum-Chemical Investigation of the $[H_6X_4O_2]^{2-}$ (X = Cl, Br) Anions," *Journal of Chemical Crystallography* 50 (2020): 69–76, https://doi.org/10.1007/s10870-019-00773-w.

48. M. Bakardjiev, J. Holub, Z. Růžičková, et al., "Transformation of Various Multicenter Bondings Within Bicapped-Square Antiprismatic Motifs: Z -Rearrangement," *Dalton Transactions* 50 (2021): 12098–12106, https://doi.org/10.1039/D0DT04225K.

49. A. J. Rosenbaum, D. H. Juers, and M. A. Juhasz, "Copper-Promoted Cyanation of a Boron Cluster: Synthesis, X-ray Structure, and Reactivity of 12-CN-*closo*-CHB_{11} H_{10}–," *Inorganic Chemistry* 52 (2013): 10717–10719, https://doi.org/10.1021/ic4015306.

50. R. M. Dziedzic, L. M. A. Saleh, J. C. Axtell, et al., "B–N, B–O, and B–CN Bond Formation via Palladium-Catalyzed Cross-Coupling of B-Bromo-Carboranes," *Journal of the American Chemical Society* 138 (2018): 9081–9084, https://doi.org/10.1021/jacs.6b05505.

51. S. Kapuściński, M. B. Abdulmojeed, T. E. Schafer, et al., "Photonic Materials Derived from the [*closo*-$B_{10}H_{10}]^{2-}$ Anion: Tuning Photophysical Properties in [*closo*-$B_{10}H_8$-1-X-10-(4-Y-NC_5H_5)]$^-$," *Inorganic Chemistry Frontiers* 8 (2021): 1066–1082.

52. S. Z. Konieczka, F. Schlüter, C. Sindorf, C. Kerpen, E. Bernhardt, and M. Finze, "Stepwise Introduction of Cyano Groups Into *Nido* - and *Closo* -Undecaborate Clusters," *Chemistry – A European Journal* 24 (2018): 3528–3538, https://doi.org/10.1002/chem.201704860.

53. C. Weetman, "Low Valent Main Group Compounds in Small Molecule Activation," in *Encyclopedia of Inorganic and Bioinorganic Chemistry* (Wiley, 2021), https://doi.org/10.1002/9781119951438.

54. E. H. Adillon and J. C. Peters, "A Carborane-Derived Proton-Coupled Electron Transfer Reagent," *Journal of the American Chemical Society* 146 (2024): 30204–30211, https://doi.org/10.1021/jacs.4c09007.

55. M. D. Marshall, R. M. Hunt, G. T. Hefferan, R. M. Adams, and J. M. Makhlouf, "Opening the B10H102-Cage to Produce B10H12(Et2S)2," *Journal of the American Chemical Society* 89 (1967): 3361–3362, https://doi.org/10.1021/ja00989a054.

56. P. R. D. Murray, J. H. Cox, N. D. Chiappini, et al., "Photochemical and Electrochemical Applications of Proton-Coupled Electron Transfer in Organic Synthesis," *Chemical Reviews* 122 (2021): 2017–2291, https://doi.org/10.1021/acs.chemrev.1c00374.

57. Y. Ashida, K. Arashiba, K. Nakajima, and Y. Nishibayashi, "Molybdenum-Catalysed Ammonia Production With Samarium Diiodide and Alcohols or Water," *Nature* 568 (2019): 536–540, https://doi.org/10.1038/s41586-019-1134-2.

58. Deposition numbers 2487180 (for ***o*-2c**), 2487178 (for ***o*-2d**), 2487177 (***o*-2e**), 2487175 (***p*-2^{Cy}**), 2487173 (***p*-2ai^{Pr}**), 2487174 (for ***p*-2a^{Cy}**), 2487179 (for ***p*-2b^{Cy}**) and 2487176 (for ***p*-2d^{Cy}**) contain the supplementary crystallographic data for this paper. Copies of this information may be obtained free of charge from The Director, CCDC, 12 Union Road, Cambridge CB2 1EY, UK (fax: +44-1223-336033; e-mail: deposit@ccdc.cam.ac.uk or www: http://www.ccdc.cam.ac.uk).

59. O. L. Tok, M. Bakardjiev, B. Štíbr, et al., "Click Dehydrogenation of Carbon-Substituted *Nido*-5,6-$C_2B_8H_{12}$ Carboranes: A General Route to *Closo*-1,2-$C_2B_8H_{10}$ Derivatives," *Inorganic Chemistry* 55 (2016): 8839–8843, https://doi.org/10.1021/acs.inorgchem.6b01386.

60. J. Holub, T. Jelínek, and Z. Janoušek, "New Multigram-Scale Preparation of 1,10-Dicarba-Closo-Decaborane," *Collection of Czechoslovak Chemical Communications* 67 (2002): 949–952, https://doi.org/10.1135/cccc20020949.

61. M. F. Hawthorne, D. C. Young, T. D. Andrews, et al., ".pi.-Dicarbollyl Derivatives of the Transition Metals. Metallocene Analogs," *Journal of the American Chemical Society* 90 (1968): 879–896, https://doi.org/10.1021/ja01006a008.

62. S. L. Holt, *Inorganic Syntheses* (John Wiley, 1983), 227.

63. T. Schaub and U. Radius, "Efficient C—F and C—C Activation by a Novel N-Heterocyclic Carbene–Nickel(0) Complex," *Chemistry – A European Journal* 11 (2005): 5024–5030, https://doi.org/10.1002/chem.200500231.

64. M. Tobisu, A. Yasutome, H. Kinuta, K. Nakamura, and N. Chatani, "1,3-Dicyclohexylimidazol-2-Ylidene as a Superior Ligand for the Nickel-Catalyzed Cross-Couplings of Aryl and Benzyl Methyl Ethers With Organoboron Reagents," *Organic Letters* 16 (2014): 5572–5575, https://doi.org/10.1021/ol502583h.

65. G. M. Sheldrick, "SHELXT-Integrated Space-Group and Crystal-Structure Determination," *Acta crystallographica Section A, Foundations and Advances* A71 (2015): 3–8.

66. M. J. Frisch and G. W. Trucks, Gaussian 16, Wallingford, CT, 2016.

67. A. D. Becke, "Density-Functional Thermochemistry. III. The Role of Exact Exchange," *Journal of Chemical Physics* 98 (1993): 5648–5652, https://doi.org/10.1063/1.464913.

68. C. Adamo and V. Barone, "Toward Reliable Density Functional Methods Without Adjustable Parameters: The PBE0 Model," *Journal of Chemical Physics* 110 (1999): 6158–6170, https://doi.org/10.1063/1.478522.

69. F. Weigend and R. Ahlrichs, "Balanced Basis Sets of Split Valence, Triple Zeta Valence and Quadruple Zeta Valence Quality for H to Rn: Design and Assessment of Accuracy," *Physical Chemistry Chemical Physics* 7 (2005): 3297, https://doi.org/10.1039/b508541a.

70. J. Tomasi, B. Mennucci, and R. Cammi, "Quantum Mechanical Continuum Solvation Models," *Chemical Reviews* 105 (1998): 2999–3094, https://doi.org/10.1021/cr9904009.

71. S. Grimme, J. Antony, S. Ehrlich, and H. Krieg, "A Consistent and Accurate Ab Initio Parametrization of Density Functional Dispersion Correction (DFT-D) for the 94 Elements H-Pu," *Journal of Chemical Physics* 132 (2010): 154104, https://doi.org/10.1063/1.3382344.

72. T. A. Keith, AIMAll (Version 19.10.12), T2019.

Supporting Information

Additional supporting information can be found online in the Supporting Information section.

Supporting File 1: The Supporting Information contains details on the synthesis, characterization, and crystal data [58] of the compounds prepared and computational details. The authors have cited additional references within the Supporting Information [59–72].

Supporting File 2: anie71935-sup-0002-Data.zip.